Bull Math Biol (2012) 74:2204–2231
DOI 10.1007/s11538-012-9753-x

ORIGINAL ARTICLE

Re-evaluating the Use of Voronoi Tessellations in the Assessment of Oxygen Supply from Capillaries in Muscle

A.A. Al-Shammari · E.A. Gaffney · S. Egginton

Received: 27 February 2012 / Accepted: 3 July 2012 / Published online: 25 July 2012

Abstract The ability to characterise capillary supply plays a key role in developing effective therapeutic interventions for numerous pathological conditions, such as capillary loss in skeletal or cardiac muscle. However, quantifying capillary supply is fraught with difficulties. Averaged measures such as capillary density or mean inter-capillary distance cannot account for the local geometry of the underlying capillary distribution, and thus can only highlight a tissue wide, global hypoxia. Detailed tissue geometry, such as muscle fibre size, has been incorporated into indices of capillary supply by considering the distribution of Voronoi tessellations generated from capillary locations in a plane perpendicular to muscle fibre orientation, implicitly assuming that each Voronoi polygon represents the area of supply of its enclosed capillary. Using a modelling framework to assess the *capillary supply capacity* under maximal sustainable conditions in muscle, we theoretically demonstrate that Voronoi tessellations often provide an accurate representation of the regions supplied by each capillary. However, we highlight that this use of Voronoi tessellations is inappropriate and inaccurate in the presence of extensive capillary rarefaction and pathological variations in oxygen tension of different capillaries. In such cases, oxygen flux trapping regions are developed to provide a more general representation of the capillary supply regions, in particular incorporating the additional influences of heterogeneity that are absent in the consideration of Voronoi tessellations.

A.A. Al-Shammari (✉) · E.A. Gaffney
Centre for Mathematical Biology, Mathematical Institute, University of Oxford, 24-29 St Giles', Oxford OX1 3LB, UK
e-mail: alshammari@maths.ox.ac.uk

A.A. Al-Shammari
Department of Mathematics, Faculty of Sciences, Kuwait University, P.O. Box 5969, Khaldiya 13060, Kuwait

S. Egginton
Centre for Cardiovascular Sciences, The University of Birmingham, Edgbaston, Birmingham B15 2TT, UK

Keywords Oxygen transport · Capillary supply · Mathematical modelling · Voronoi tessellations · Flux trapping regions

1 Introduction

Aerobic respiration for virtually all mammalian cells is contingent on a local capillary bed establishing an adequate partial pressure gradient for oxygen (O_2) diffusion to drive its transport. This in turn depends on numerous factors including the distribution, perfusion, and tortuosity of capillaries; mitochondrial locations; variations in the capillary blood flow and haematocrit; the interstitial and cellular geometry; the levels of facilitated diffusion; the interaction of haemoglobin and oxygen; tissue temperature and intracellular composition (Hudlicka et al. 1992).

Understanding oxygen transport at the cellular level poses outstanding difficulties, for instance quantifying the link between cellular demand and capillary supply, whilst current experimental interrogations at the scale of several microns are laborious with limited resolution. Consequently, numerous theoretical models have been developed to give insight into microvascular oxygen transport, as initiated by Krogh and Erlang's 1919 cylindrical model (Krogh 1919). This has become the basis for numerous subsequent modelling explorations despite its limitations (Kreuzer 1982), culminating in relatively recent 3D microvascular oxygen transport modelling studies (Beard and Bassingthwaighte 2001; Goldman and Popel 2000; Secomb et al. 2004).

However, skeletal and cardiac muscles exhibit a relatively simple histological structure, with capillaries typically running parallel to muscle fibres, as illustrated in Fig. 1. Thus, such tissues are not only important in their own right, but also offer an opportunity for the study of tissue oxygenation without detailed three dimensional geometrical complexity, removing the laborious requirement of capturing accurately digitised tissue histology (Janacek et al. 2011), especially for studies demanding high statistical significance. Consequently, there have been numerous studies quantifying 2D capillary and fibre distributions in skeletal muscle. While this structural information cannot account for the regulation of capillary blood flow, there have been numerous attempts to exploit such data in the characterisation of muscle capillary supply capacity and its regulation (Clark et al. 1989; Hoofd et al. 1989, 1990; Hoofd 1995; Wang and Bassingthwaitghte 2001; Salathe 2003; Burrowes et al. 2004; Safaeian et al. 2011).

Standard measures of capillary supply capacity based on muscle structural data consider scalar indices such as capillary density (CD), capillary-to-fibre ratio (C:F), or mean inter-capillary distance (ICD) (Egginton and Ross 1989, 1992). However, these are scale-dependent indices as they can be greatly affected by muscle fibre growth (or atrophy) when tissue is subjected to local remodelling (Ahmed et al. 1997). Thus, they only resolve global details, neglecting the local geometry of the underlying capillary distribution (see Fig. 1) and potentially important cellular level details such as a local reduction in capillary numbers or local pockets of ischaemia (Hargreaves et al. 1990).

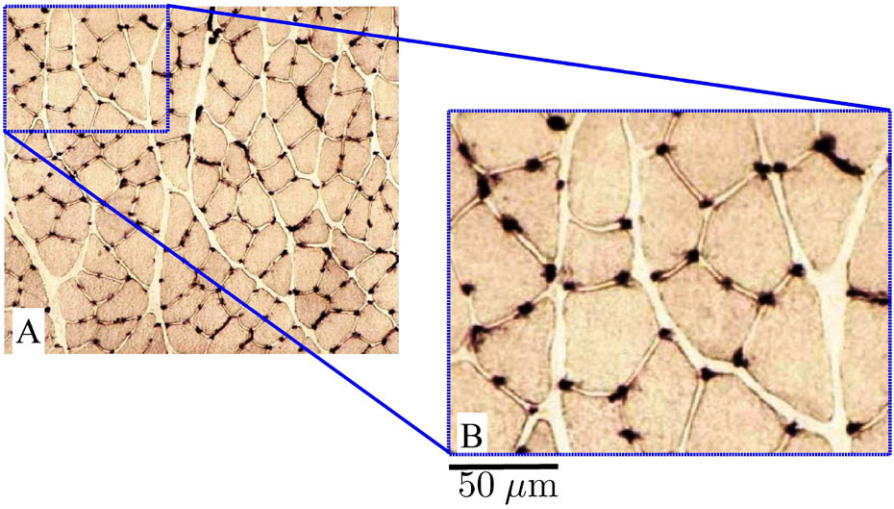

Fig. 1 (**A**) typical tissue cross section of rat skeletal muscle (*m. extensor digitorum longus*) with capillary location identified by alkaline phosphatase staining. (**B**) An expanded region of the original image. The *dark structures* are capillaries, the *lighter objects* are muscle fibres, and the *lightest region* is the interstitial space. Note the heterogeneity of intercapillary distances between adjacent vessels, in part reflecting heterogeneity of cell size in the host tissue (Egginton et al. 1988; Egginton and Ross 1989)

This has motivated numerous studies which attempted to generalise measures of muscle capillary supply in an attempt to provide discriminatory indices that incorporate aspects of the local capillary distribution and fibre size for use in comparative studies. Hence, the region oxygenated by an individual capillary, also referred to as the capillary supply region or domain, is of immediate interest. While Krogh and Erlang's influential model (Krogh 1919) represented the capillary supply region as a cylinder concentric with the capillary, the inability to tessellate space with cylinders has motivated more sophisticated approaches, even in 2D muscle models. In particular, in the cross section of the muscle, as illustrated in Fig. 1, Voronoi polygon representations for the capillary oxygen supply regions have often been considered (Turek et al. 1986; Wüst et al. 2009a, 2009b; Scott et al. 2009; Degens et al. 1992, 2002, 2006, 2008; Karch et al. 2005; Batra and Rakušan 1991; Batra et al. 1991; Rakušan et al. 1992, 1994, 2001a, 2001b; Rakušan and Turek 1985, Sladek et al. 1996; Tomanek et al. 1990, 1991; Turek et al. 1987, 1992; Heron and Rakušan 1994; Koyama et al. 1998; Koyama and Taka 2010).

In detail, a Voronoi polygon is an area within a tissue cross section that encloses a capillary whereby every tissue point is closer to this capillary than to any other, as illustrated in Fig. 2. Its adoption as a representation of capillary supply region can be attributed to its ease of use and the absence of detailed parameter estimation. Thus, of key interest are the numerous choices of indices based on the Voronoi polygons extracted from tissue sample observations to estimate capillary supply capacity (Egginton and Ross 1989). Examples of these indices include local capillary-to-fibre ratio (LCFR) and local capillary density (LCD) (Hargreaves et al. 1990; Egginton and Ross 1989), which have the potential to reveal changes in capillary

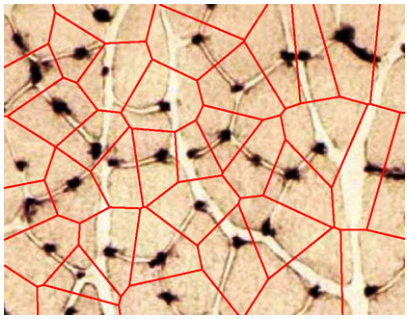

Fig. 2 The Voronoi polygon tessellation superimposed on the magnified tissue cross section from Fig. 1

supply capacity following microvascular remodelling as well as disruptions in the regulation between angiogenesis and oxygen demand (Batra and Rakušan 1991; Batra et al. 1991; Degens et al. 1992, 2002, 2006, 2008; Egginton et al. 2001; Wüst et al. 2009a; Scott et al. 2009; Karch et al. 2005). This is especially pertinent in the context of ischaemia due to disease and associated therapeutic interventions, which include strength training exercise (Deveci and Egginton 2002; Suzuki et al. 2000), endurance exercise (Ahmed et al. 1997; Scott et al. 2009), electrical stimulation (Ebina et al. 2002), and alterations in temperature (Egginton et al. 2001; Egginton 2002).

The first to effectively explore Voronoi polygons were Gonzalez-Fernandez and Atta (1972). They considered capillary geometries that led to various regular tessellations of the plane, including hexagonal tessellations. While Voronoi polygons will represent capillary supply regions for perfectly symmetric capillary distributions within tissue of homogeneous oxygen consumption, a sufficiently pronounced asymmetry will, in general, lead to a breakdown in the correlation between Voronoi polygon and capillary supply regions (Egginton and Gaffney 2010). However, it is still unknown to what extent introducing physiologically representative asymmetries in capillary distribution influence the quality of Voronoi polygons in capturing capillary supply capacity. Wang and Bassingthwaighte (2001) explored this question and criticised the usage of Voronoi polygons for asymmetrical capillary arrangements, concluding that they are inappropriate. However, the study was based upon a mathematical analysis that necessitated the consideration of un-physiologically low capillary densities within the region of interest. Hence, this still leaves the question of whether Voronoi polygon indices are appropriate in the physiological setting. Therefore, our objective has been to explore a general model of oxygen transport under maximal sustainable conditions in tissue, characterising where and when Voronoi polygon indices are likely to accurately represent the underlying transport processes, while also characterising an alternative index of capillary supply capacity in muscle.

2 Methods

The cross sections in Figs. 1, 2 are microscopy images of rat skeletal muscle, *m. extensor digitorum longus*, prepared via flash freezing in liquid nitrogen-cooled isopentane and cryostat sectioned at -20 °C with the capillary location identified using alkaline phosphatase staining (Egginton et al. 2001).

3 Key Definitions

We consider a cross section of tissue, as in Fig. 2 where the capillary locations are represented by a single point, e.g. the centroid of each capillary in the image plane of the muscle cross section. Let N_c denote the number of capillaries, and $\mathbf{x}_i$ denote the position of the ith capillary with D representing the global domain.

3.1 Voronoi Polygons

The Voronoi polygon containing the ith capillary with centre $\mathbf{x}_i$ is the set

$$V_i = \left\{ \mathbf{x} \,\middle|\, \mathbf{x} \in D; |\mathbf{x} - \mathbf{x}_i| \leq |\mathbf{x} - \mathbf{x}_k|,\ k \neq i \right\}. \tag{1}$$

This definition states that the Voronoi polygon associated with the ith capillary is the closure of the set of points which are closer to capillary i than any other capillary. Note that the V_i tessellate D.

3.2 Trapping Regions

For a given capillary with a positive oxygen flux at its boundary (vessel wall), the *trapping region* is the smallest domain which contains the capillary, with zero flux conditions on its boundary. Thus, for a solution of the model equations for tissue oxygen partial pressure p, the trapping region $D_i \subseteq D$ of a capillary with centre $\mathbf{x}_i$, with outward pointing normal $\mathbf{n}_i$ is defined to be the smallest domain within a closed boundary containing $\mathbf{x}_i$ and satisfying

$$\partial D_i = \{ \mathbf{x} \in D \,|\, \mathbf{n}_i \cdot \nabla p = 0 \}. \tag{2}$$

In addition, when the model prediction for oxygen flux at the capillary wall is negative, the trapping region is empty. Finally, when a mixture of positive and negative oxygen fluxes is present at the capillary wall, the boundary of the trapping region can also consist of the capillary boundaries so that each trapping region gives the predicted region of oxygen supply for each capillary.

Clearly, the above is a model-dependent definition. Each D_i yields the area surrounding a capillary where the outward flux due to the ith capillary is balanced by inward flux due to all the neighbouring capillaries of contiguous supply regions. In addition, the regions D_i need not tessellate D; if they do not, then there is at least one region in D which does not receive any oxygen from any capillary, which is a mathematical but not physiological possibility.

By construction, D_i represents the region of supply of each capillary, according to the model used to determine the oxygen partial pressure p in tissue. When Voronoi polygons are used to represent the region of capillary supply, the validity of this assumption dictates the validity of capillary supply capacity indices. Thus we are interested in delimiting when the ith Voronoi polygon, V_i, yields a good approximation to the ith trapping region, D_i.

4 Modelling Framework

In the following, we develop a detailed model for O_2 transport under maximal sustainable conditions in muscle tissue, as exemplified by the typical tissue cross section presented in Fig. 1, where the length scale of a capillary cross-section is of order 2–4 μm.

4.1 2D Formulation

We examine O_2 transport in a two-dimensional domain representing a cross section of skeletal muscle tissue. Perpendicular to this domain, an array of small capillaries of circular cross-sectional shape supply the tissue with O_2 through passive diffusion (Popel 1989). Axial diffusion of O_2 in tissue can be neglected as long as the ratio of characteristic intercapillary distance (10^1 μm) to capillary length (10^3 μm) is sufficiently small, an assumption that is supported experimentally when myoglobin-facilitated diffusion is limited (Gayeski and Honig 1988; Kreuzer 1982). In turn, myoglobin facilitation can be neglected when the tissue partial pressure, PO_2, is well above $p_{\mathrm{Mb},50} = 2$–5 mmHg (Popel 1989; Goldman and Popel 2000), where $p_{\mathrm{Mb},50}$ is the oxygen partial pressure at 50 % saturation of myoglobin.

4.1.1 Governing Equations

Excluding un-physiologically high O_2 concentrations, the oxygen flux, $\mathcal{J}$, can be assumed to be proportional to the gradient of O_2 concentration, c, via Fick's first law, $\mathcal{J} = -D\nabla c$, where D is the O_2 diffusion coefficient in muscle tissue. By Henry's law, we have $c = \alpha p$, where p is the tissue partial pressure of O_2 (PO_2) and α is the coefficient of tissue O_2 solubility. Thus, in the absence of axial and myoglobin-facilitated diffusion, conservation principles give

$$\frac{\partial(\alpha p)}{dt} = \nabla \cdot [\alpha \mathcal{D} \nabla p] - \mathcal{M}(p), \tag{3}$$

where $\mathcal{M}$ is the rate of O_2 consumption in tissue. Note that, for a timescale of hours, this process is in *quasi-steady state* (see Table 1). Moreover, we assume that $\mathcal{M}$ is constant and uniform, and thus we implicitly assume that oxygen supply is sufficient to ensure that uptake is at saturation levels. As detailed by Wilson et al. (1988), this necessitates that tissue PO_2 is above a critical value, denoted p_{critical}, which is approximately 0.5–1.0 mmHg (Wilson et al. 1988; Goldman 2008). Thus, for model consistency with the assumption of limited myoglobin facilitation, we only consider parameter scenarios with $p > p_{\mathrm{Mb},50} > p_{\mathrm{critical}}$ (Richardson et al. 1995, 2001), and hence $\mathcal{M}(p) = \mathcal{M}_0$, a constant metabolic demand. This likely pertains to a range of tissue activity from rest to sustainable aerobic activity in muscle, i.e. endurance exercise.

The domain geometry is typically obtained by considering a circular tissue cross section and then re-scaling onto the unit disk, $\mathbb{D}^1$. Capillaries are assumed to possess an area, C_i, and a boundary, ∂C_i. Therefore, we seek to investigate PO_2 in a region

Table 1 Except for number of capillaries, parameter values *above the line* are taken from Goldman and Popel (2000), while those *below the line* are derived values. The number of capillaries is estimated from capillary densities. Note that $\rho\mathcal{D} \sim 3\ \mathrm{s}^{-1}$ indicating that the transport equation, Eq. (3), is in quasi-steady state for timescales of hours and longer, as the evolution of the system toward the steady state is driven by the timescale emerging from diffusion and the intercapillary distance $\sim 1/\rho^{1/2}$

Parameter	Symbol	Value
Tissue O_2 solubility	α	3.89×10^{-5} ml O_2 ml^{-1} mmHg^{-1}
Tissue O_2 diffusivity	$\mathcal{D}$	2.41×10^{-5} cm^2 s^{-1}
Tissue O_2 consumption	$\mathcal{M}_0$	1.57×10^{-4} ml O_2 ml^{-1} s^{-1}
Mass transfer coefficient	k	4.0×10^{-6} ml O_2 s^{-1} cm^{-2} mmHg^{-1}
Average intra-capillary partial pressure	p_{cap}	20 mmHg
Capillary radius	r	1.8 μm
Capillary density	ρ	1400 mm^{-2}
Number of capillaries	N_c	612
Length scale	L	7.46×10^{-2} cm
Transfer coefficient	κ	318.32 *non-dimensionalised*
O_2 consumption	μ	18.64 *non-dimensionalised*

of the unit disk that excludes the capillary lumina, $C := \mathbb{D}^1 \backslash \bigcup_i C_i$. Thus, our model oxygen transport equation is reduced to

$$\alpha\mathcal{D}\nabla^2 p - \mathcal{M}_0 = 0 \quad \text{in } C. \tag{4}$$

4.1.2 Boundary Conditions

We consider the partial pressure and flux of O_2 at the blood-tissue interface of the capillary wall. Since it is well known that there is a finite intra-capillary resistance to blood-tissue O_2 transport (Eggleton et al. 2000), we can utilise the *mass transfer coefficient* (Fletcher 1978; Goldman and Popel 2000), k, which gives a quantitative measure for mass O_2 transport from haemoglobin and through the capillary-tissue interface. Letting each capillary have an *inward* normal, $\mathbf{n}_i$, such that $\mathbf{n}_i$ is outward to the region C, conservation of mass at the capillary wall requires

$$k(p_{\mathrm{cap}} - p) = \mathcal{J}_{\mathrm{wall}} = -\alpha\mathcal{D}\frac{\partial p}{\partial r} = \mathbf{n}_i \cdot \alpha\mathcal{D}\nabla p \quad \text{on } \partial C_i, \tag{5}$$

where p_{cap} is the transversally-averaged partial pressure of O_2 in blood (intra-capillary), $\mathcal{J}_{\mathrm{wall}}$ is the capillary-tissue O_2 flux, p is the partial pressure of O_2 at the external capillary wall, and r is the radial coordinate. Additionally, a no-flux boundary condition is imposed at the outer boundary of the tissue, effectively the muscle fascicle, to signify no exchange across it

$$\left.\frac{\partial p}{\partial r}\right|_{r=1} = 0. \tag{6}$$

Even when the domain boundary within the model does not represent a physiological fascicle, the use of this no-flux boundary condition is still justifiable within

the context of our study, as we justify a posteriori that perturbing this condition does not influence the system behaviour away from the boundary. In particular, our investigation will be based on a representative internal region of the tissue cross section in which boundary effects become practically negligible, as described below.

4.1.3 Streamlines

Central to the numerical computation of trapping regions of oxygen partial pressure, PO_2, is the concept of a *streamline*. A streamline for a vector field is a curve, the direction of which coincides at each point with the direction of the vector field; that is, at all locations it is tangential to the vector field. We consider the streamlines associated with the gradient of the oxygen partial pressure, ∇p, and note that these are the trajectories (integral paths) given by

$$\frac{d\mathbf{x}}{ds} = -\nabla p \tag{7}$$

for all $\mathbf{x} = (x, y)$ in the physical domain, with s parameterising the integral path. Therefore, a trapping region is an area of the muscle reached by streamlines emerging from a given capillary and hence streamlines can be used to determine trapping region boundaries from modelling predictions of oxygen partial pressures, as detailed in Appendices A.4 and B.

4.1.4 Non-dimensionalisation

We non-dimensionalise the spatial scales and partial pressure. With N_c capillaries in a disk of diameter L and an average density of ρ/mm^2, we have $\pi(L/2)^2 = N_c/\rho$, i.e. $L = \sqrt{\frac{4Nc}{\pi\rho}}$. This is used along with p_{cap} to non-dimensionalise our model equation and boundary conditions. Hence, the non-dimensional problem to solve is

$$\nabla^2 p - \mu = 0 \quad \text{in } C, \tag{8}$$

$$\left.\frac{\partial p}{\partial r}\right|_{r=1} = 0, \qquad \mathbf{n}_i \cdot \nabla p = \kappa(\eta_i - p) \quad \text{on } \partial C_i, \tag{9}$$

$$\mu = \frac{L^2 \mathcal{M}_0}{\mathcal{D}\alpha p_{\text{cap}}}, \qquad \kappa = \frac{Lk}{\mathcal{D}\alpha}. \tag{10}$$

Here, $\mu > 0$ is the non-dimensionalised metabolic demand, $\kappa > 0$ is the non-dimensionalised transfer coefficient, and η_i is the non-dimensionalised O_2 partial pressure at the ith capillary wall. Note that p is non-dimensionalised with the maximum p_{cap} such that the ith capillary has a unit non-dimensional partial pressure when p_{cap} is uniform or a value η_i otherwise.

4.1.5 Capillary Distributions

For our model, capillaries are initially placed based on a hexagonal array to mimic the approximate distribution of capillaries in select oxidative muscles. The heterogeneity

in capillary placement is introduced by a *perturbative* method, with the addition of a random vector to the position of each capillary. The random vector has a magnitude that is a fraction of the hexagonal array side length, s, while its direction is based on an angle, ϕ, that is uniformly distributed on $[-\pi, \pi)$. We refer to perturbations via the parameter β defined by the relative magnitude of the random vector to the hexagonal array side length, and consider it as a measure of heterogeneity, with larger values indicating more heterogeneous arrangements. Hence, we take

$$\mathbf{x}_{\text{perturbed}} = \mathbf{x}_{\text{original}} + \beta s(\cos\phi, \sin\phi), \quad \phi \in [-\pi, \pi). \tag{11}$$

We consider regular, perturbed, random, and real distributions of capillary arrangements. For regular and perturbed distributions, we initially place N_c capillaries on a hexagonal array. For regular distributions, the capillaries are not perturbed, while for *small*, *medium* and *large* perturbations we then generate the capillary locations using Eq. (11), respectively, taking $\beta = 0.25, 0.50, 1.00$. In addition, random distributions are generated with a uniform probability per unit area; in contrast, *real* distributions are based on a muscle image cross section where the capillary arrangement is taken from a rat *extensor digitorum longus* muscle image rescaled onto the unit disk. Finally, we consider three capillary arrangements: *slight* and *severe* rarefactions, and *rarefied* muscle. To generate the rarefied distributions, capillaries are simply removed from a capillary arrangement that is either randomly generated or extracted from a rat EDL muscle.

4.2 Model Properties

It can be easily shown that our model for the oxygen partial pressure possesses a unique solution, as detailed in Appendix A.1.

4.2.1 Nature of Trapping Regions

The area of the ith trapping region, D_i, is given by

$$A_i = \frac{\kappa}{\mu} \oint_{\partial C_i} (\eta_i - p)\, ds, \tag{12}$$

assuming the flux of oxygen at the capillary boundary is always from the capillary into the surrounding tissue, as derived in Appendix A.3. We note that this provides the simplest and most accurate means to calculate trapping region areas from the numerical solution of the partial pressure. While the resulting area does not require the geometric determination of the trapping region, the trapping region geometries are also determined as described in Appendix B.3.

4.2.2 Parameter Values

Our parameter values are given in Table 1 and based upon those presented by Goldman et al. (2000), which in turn are based on numerous experiments (Altman and Dittmer 1971; Bentley et al. 1993; Christoforides et al. 1969; Dong 1997;

Ellsworth et al. 1988; Honig and Gayeski 1982; Clark et al. 1985; Jürgens et al. 1994; Mahler et al. 1985; Meng et al. 1993; Sullivan and Pittman 1984). The length scale, L, can be derived by assuming the 612 capillaries in the unit disk have a dimensional density of 1400 mm^{-2} (Goldman and Popel 2000). Although rat EDL muscle has generally lower capillary density values, depending on animal mass and adaptation, the capillary density we use is typical for a cardiac muscle. The use of such scalings is justified in the sensitivity analysis we present in Appendix C. In addition, we briefly consider variations in p_{cap} within a tissue for one of the simulations below. Due to possible experimental errors in estimating these parameters and natural variations, we also explore the influence of parameter variations in detail within Appendix C.

4.2.3 Model Limitations

Assuming a constant metabolic demand entails the implicit hypothesis that the tissue is never subjected to sufficiently low O_2 levels (hypoxia) such that its mitochondria would be unable to extract O_2 at the maximal rate (Schumacker et al. 1993; Wilson et al. 1988). In particular, in the case of a uniform capillary supply, p_{cap} can be chosen in our model such that the tissue PO_2 values do not fall below 5 mmHg, thus giving a maximal O_2 uptake and minimal myoglobin facilitation. Indeed, in the presence of very low O_2 levels ($p < 0.50$ mmHg), metabolic demand may have a partial pressure dependence in accordance with Michaelis–Menten kinetics (Popel 1989; Wilson et al. 1988) and the influence of myoglobin may become significant. Further, we have assumed that the muscle fibre uptake of O_2, $\mathcal{M}_0$, is uniform, although adjacent muscle fibres may be of varying oxidative demands; this additional source of heterogeneity is neglected here and will be explored in a subsequent study. Finally, since our model predicts the behaviour of this system within the limits of capillary supply capacity and no-axial convection and diffusion, its results are currently restricted to 2-dimensional muscle cross sections, but in principle extendable to 3-dimensional images.

5 Results

We solve Eqs. (8)–(9) for the oxygen partial pressure, enabling a derivation of the streamlines via Eq. (7), and a subsequent determination of trapping region areas using Eq. (12) and the trapping region geometries using the numerical methodologies in Appendix B.

5.1 Definitions

5.1.1 The Region of Interest

Motivated by experimental practice, we introduce the *region of interest*, a square box within the disk and concentric with it, which is used to select capillaries for consideration. The edges of this region are further from the edge of the domain than the

Table 2 Statistical measures for all capillaries i in the region of interest. These are used to evaluate the quality of Voronoi polygons. Here, D_i and V_i are the ith trapping region and Voronoi polygon, respectively, and T_i is their intersection. Here, *std* refers to the standard deviation, *mean* denotes the arithmetic mean, and *area* corresponds to the non-dimensional area. See Sect. 5.4 for a discussion of these measures in the context of our oxygen transport simulations

Statistic	Definition
Normalised mean of difference	$\Delta_{\text{mean}} := \frac{\text{mean}[area(D_i) - area(V_i)]}{\text{mean}[area(D_i)]}$
Normalised standard deviation of difference	$\Delta_{\text{std}} := \frac{\text{std}[area(D_i) - area(V_i)]}{\text{mean}[area(D_i)]}$
Normalised mean of intersection	$\cap_{\text{mean}} := \frac{\text{mean}[area(T_i)]}{\text{mean}[area(D_i)]}$
Normalised standard deviation of intersection	$\cap_{\text{std}} := \frac{\text{std}[area(T_i)]}{\text{mean}[area(D_i)]}$
Normalised standard deviation of Voronoi polygons	$\square_{\text{std}} := \frac{\text{std}[area(V_i)]}{\text{mean}[area(V_i)]}$
Normalised standard deviation of trapping regions	$\bigcirc_{\text{std}} := \frac{\text{std}[area(D_i)]}{\text{mean}[area(D_i)]}$
Mean ratio	$\mathcal{R} := \text{mean}\left[\frac{area(V_i)}{area(D_i)}\right]$

intercapillary distance as the objective is to remove domain boundary artefacts, as can be confirmed a posteriori. The upper and left-hand sides of the square are identified as *inclusion lines*, and the lower and right-hand sides are, in contrast, *exclusion lines* (Egginton 1990). A capillary domain of influence is counted as within the region of interest if it falls entirely within the box, or if it falls partly within the box and overlaps inclusion lines *only*. To ensure robust statistical measures we consider identical populations of capillaries, using Voronoi polygons *only* to represent the capillary domain of influence when considering the inclusion criteria for the region of interest. Furthermore, these criteria allow the tessellation of multiple regions of interest without double counting artefacts, so that it may represent the basis for considering transport processes at higher scales.

5.1.2 Definition of Statistics

In Table 2, we define the statistical measures that will be used. These utilise D_i and V_i, the ith trapping region, and Voronoi polygon, as two-dimensional domains, respectively, within the region of interest and T_i, their intersection. For a tissue cross section containing 204 capillaries, the region of interest typically includes about 50 capillaries which are used to generate statistics, though we can obtain a smaller sample in the case of rarefaction. In Table 3, we present the statistics defined in Table 2 together with area correlation coefficients, $\mathcal{CC}$, for various capillary arrangements.

5.2 Oxygen Densities, Voronoi Polygons, Trapping Regions, and Histograms

5.2.1 Oxygen Partial Pressure

The range of PO_2 is an increasing function of heterogeneity, with the widest range and lowest PO_2 found in severe rarefaction and heterogeneous capillary PO_2 (Figs. 3

Table 3 Statistics determined from areas of Voronoi polygons and trapping regions for different capillary arrangements and parameter regimes. An entry denoted by * denotes cases where statistics are not applicable. The area correlation coefficient, $\mathcal{CC}$, is ill-defined for hexagonal arrays since all areas are the same, and hence their standard deviation is null. Nonetheless, it is clear that Voronoi polygon areas provide exceedingly good estimates of trapping region areas in this case. Similarly, the occurrence of zero area trapping regions for heterogeneous capillary PO_2 entails the mean ratio $\mathcal{R}$ is ill-defined in this case. An entry of # highlights that the statistics require more complex algorithms for quantitatively characterising all trapping regions, due to non-uniform p_{cap}, as detailed in Appendix B.3. For such cases, we have used Eq. (12) to compute trapping region areas noting that the capillaries with fluxes solely into the blood compartment automatically possess zero area trapping regions. The more complex cases of trapping regions which share part of a boundary with a capillary possessing fluxes in both directions across its wall are not observed in the example of inhomogeneous p_{cap} considered

Capillary arrangement	Δ_{mean}	Δ_{std}	$\cap_{mean}$	$\cap_{std}$	$\mathcal{CC}$	$\square_{std}$	$\bigcirc_{std}$	$\mathcal{R}$
Hexagonal	0.0448	0.0093	0.9991	0.0084	*	0	0.0113	0.9991
25 % perturbation	0.0805	0.0940	0.9498	0.1026	0.9508	0.1504	0.0678	0.9474
50 % perturbation	0.1140	0.1495	0.9073	0.1880	0.9503	0.2609	0.1267	0.8988
100 % perturbation	0.1690	0.2034	0.8841	0.2502	0.9530	0.3574	0.1895	0.8689
Slight rarefaction	0.2094	0.3071	0.8426	0.2816	0.9322	0.4714	0.2193	0.8247
Severe rarefaction	0.2919	0.4451	0.8104	0.4303	0.9399	0.6853	0.3820	0.7844
Rarefied muscle	0.1973	0.3057	0.8336	0.3594	0.9527	0.58	0.346	0.8223
Random	0.1631	0.2093	0.8803	0.2638	0.9180	0.3785	0.2164	0.8680
Muscle image	0.1501	0.1548	0.9297	0.1764	0.9483	0.2529	0.1411	0.9241
Heterogeneous p_{cap}	0.6215	0.5682	#	#	0.1047	0.2791	0.5615	*

and 6(a)). Some capillaries act like sinks for oxygen when the local O_2 levels are higher than the capillary supply, even though the range of capillary partial pressures was restricted to 20–30 mmHg (Fig. 4(i)).

5.2.2 Voronoi Polygons and Trapping Regions

Boundaries of Voronoi polygons are indistinguishable from those of trapping regions in the case of perfectly symmetrical capillary arrangement (Fig. 4(a)). This is not the case for the other arrangements where boundary deviations become more pronounced with increasing heterogeneity (Figs. 4(b)–(h) and 6(b)). In the case of non-uniform capillary PO_2 (Fig. 4(i)), such boundary deviations are much more pronounced, despite the fact the range of capillary partial pressures was limited.

In addition, the exterior no-flux boundary condition has been perturbed to incorporate a small sinusoidal flux of the form

$$\frac{\partial p}{\partial r} = \varepsilon \cos\theta$$

where $|\varepsilon| \leq 0.1$ to confirm that the trapping regions within the region of interest did not differ to any significant extent (results not shown). This confirms that the modelling predictions are insensitive to details of the boundary condition at the domain's external perimeter.

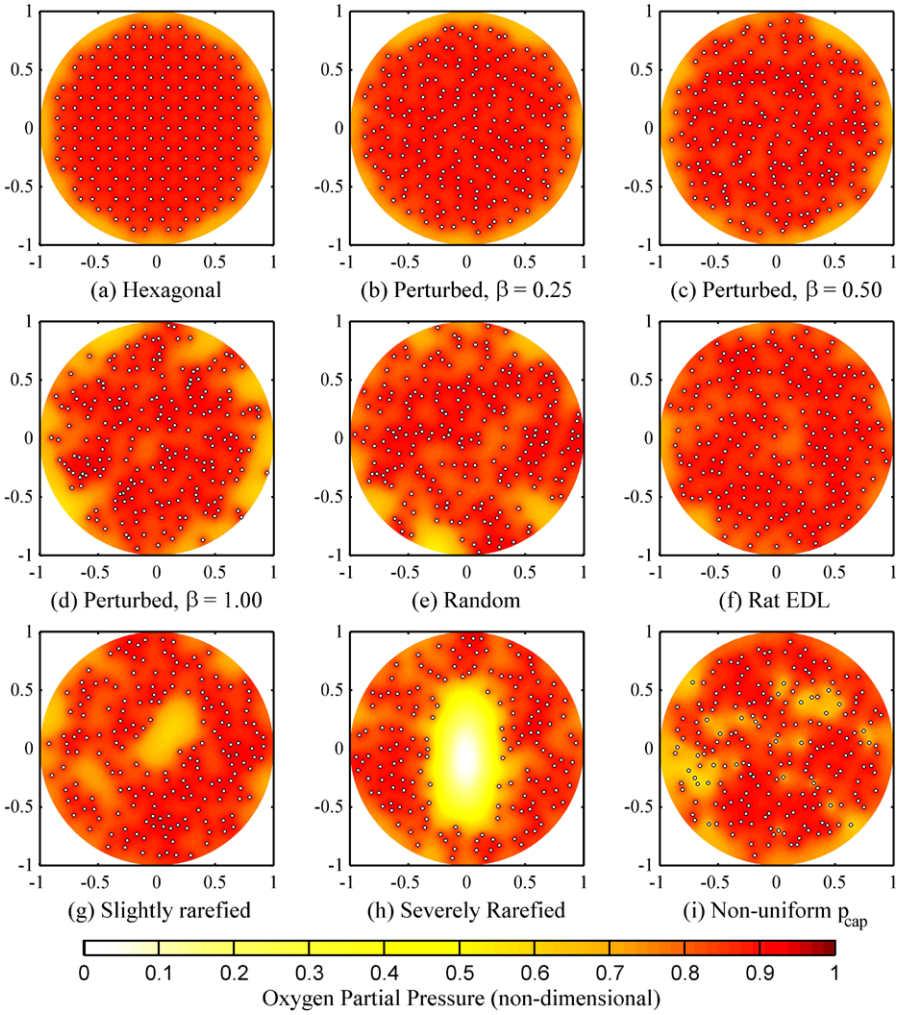

Fig. 3 Spatial distribution of oxygen partial pressure (non-dimensional units), with capillaries as small white holes

5.2.3 Frequency Histograms

Frequency histograms for the areas of the trapping regions and Voronoi polygons confirm that distributions are narrower for more homogeneous capillary arrangements. In all cases, trapping regions show narrower distributions and higher peaks than Voronoi polygons. In particular, the cases of capillary rarefaction exhibit the fattest tails with distinctive left-skewed distributions (Figs. 5 and 6(c)).

5.3 Qualitative Observations and Correlations

Voronoi polygons describe the behaviour of trapping regions with an excellent agreement for a hexagonal array of capillaries (Fig. 4(a)). In this case, boundaries of

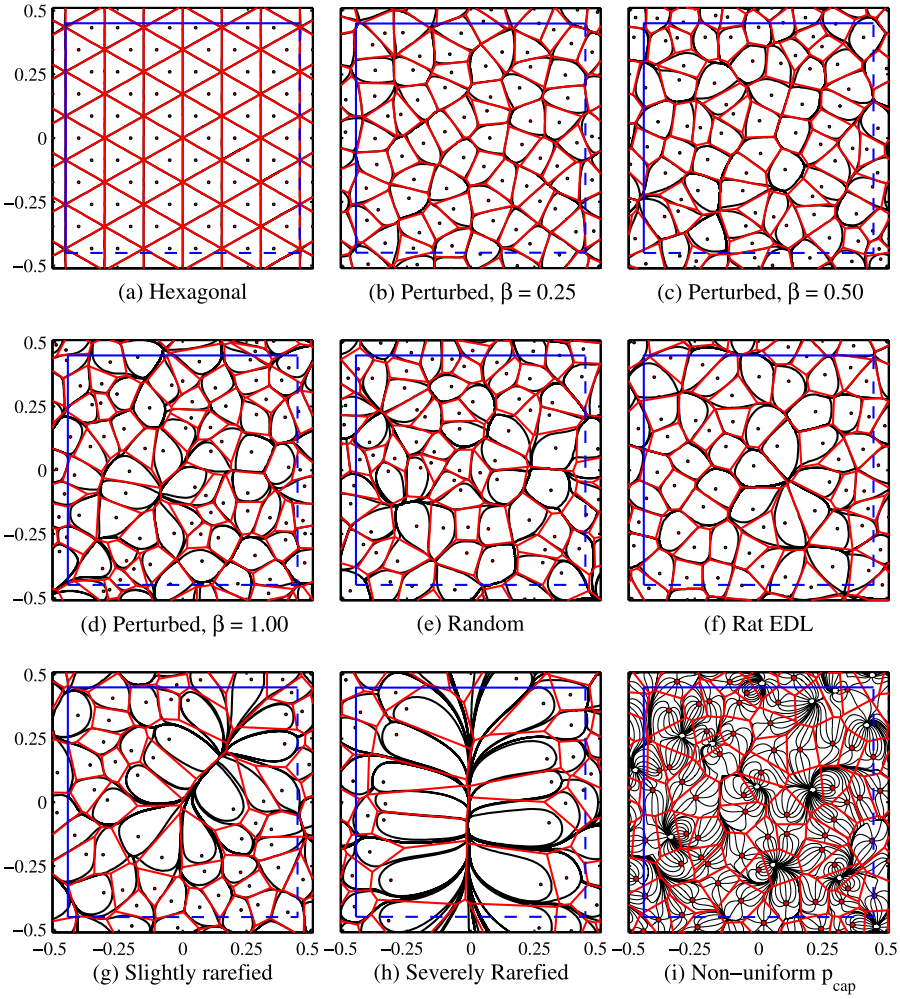

Fig. 4 (**a**)–(**h**) Trapping region boundaries (*black/dark*) and Voronoi polygons (*red/light*) in the region of interest (*blue/dark square*: *solid left/top edges* and *dashed right/bottom edges*) for various capillary distributions. (**i**) This plot represents a 50 % perturbed distribution of capillaries with heterogeneous capillary tension, p_{cap}. We have used two different p_{cap} values: $p_{\text{cap}} = 10$ mmHg for 30 randomly chosen capillaries, and $p_{\text{cap}} = 20$ mmHg for the rest. Streamlines (*black/dark*) emanate from capillaries acting as O_2 sources (*red-filled disks*), whereas the remaining capillaries (*white disks*) act entirely as receiving ends of PO_2 flux lines, thus possessing a zero area for O_2 supply

Voronoi polygons coincide with trapping regions. In particular, given the fact that Voronoi polygons should perfectly match capillary supply regions when O_2 uptake is saturated and the capillary arrangement is symmetric, this agreement further confirms that domain boundary effects can be neglected within a region of interest. However, as the heterogeneity in capillary distribution is increased, the boundaries of trapping regions are seen to deviate slightly from Voronoi polygons (Figs. 4(b)–(f)). Despite this, Voronoi polygons provide a reasonable qualitative approximation to trapping re-

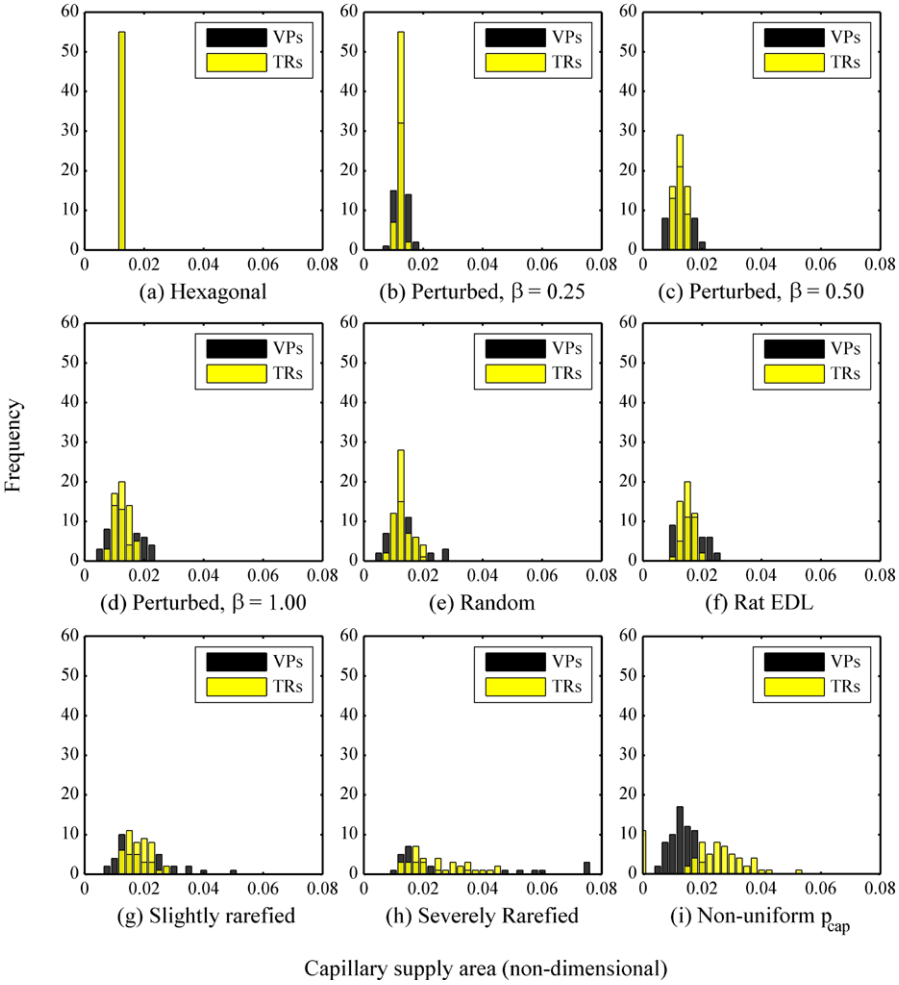

Fig. 5 Frequency distributions of areas for Voronoi polygons (VPs) and trapping regions (TRs) within the region of interest. Histograms of the areas of Voronoi polygons are given by *black/dark bars* and trapping regions by *light bars*. Overlapping histograms are of *intermediate shading*. The *horizontal axis* represents non-dimensional areas and the *vertical axis* shows frequency of occurrence, where the heights of the bars sum to the number of capillary domains included in region of interest

gions in all cases. Most of the area histograms of Voronoi polygons coincide with those of trapping regions, but as heterogeneity is increased an extended (fat) tail begins to emerge for the Voronoi polygon histograms, whereas histograms of trapping regions remain relatively centralised, thus Voronoi polygons can exaggerate extremes of capillary supply areas.

With capillary rarefaction, Voronoi polygon boundaries show larger deviations from trapping regions (Figs. 4(g)–(h) and 6(b)), in addition to a more pronounced deviation in shape and distribution of Voronoi polygon areas (Figs. 5(g)–(h) and 6(c)). These polygons deviate ever more extensively from their associated trapping regions

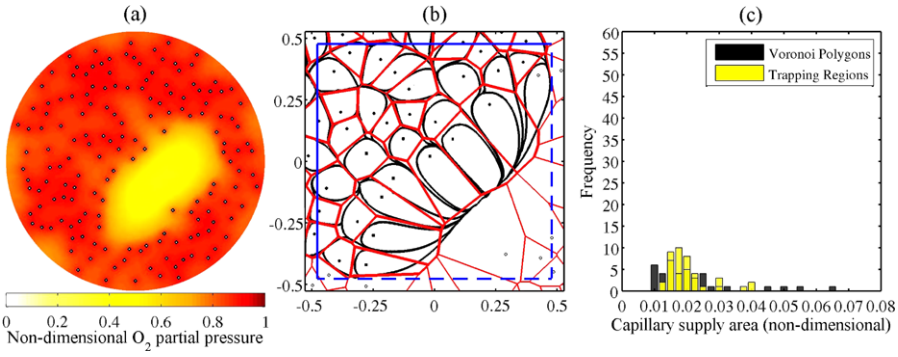

Fig. 6 Simulations for rarefied rat EDL muscle: (**a**) Spatial distribution of oxygen partial pressure (non-dimensional units), with capillaries as small white holes. (**b**) Trapping region boundaries (*black/dark*) and Voronoi polygons (*red/light*) in the region of interest (*blue/dark square*: *solid left/top edges* and *dashed right/bottom edges*). (**c**) Frequency distributions of areas for Voronoi polygons (VPs) and trapping regions (TRs) within the region of interest. Histograms of the areas of Voronoi polygons are given by *black/dark bars* and trapping regions by *light bars*. Overlapping histograms are of *intermediate shading*. The *horizontal axis* represents non-dimensional areas and the *vertical axis* shows frequency of occurrence, where the heights of the bars sum to the number of capillary domains included in region of interest

as the severity of rarefaction is increased. In addition, a simple comparison reveals that higher degrees of rarefaction severity are accompanied by a smaller number of oxygen minima (Fig. 3(c), (f) *vs.* Figs. 3(g)–(h) and 6(a)). Finally, the influence of rarefaction on distant capillaries reveals that both non-neighbouring and nearest trapping regions expand further in the direction of rarefaction while, in contrast, only the nearest Voronoi polygon neighbours compensate for rarefaction (Figs. 4(c), (f)–(h) and 6(b)).

In the case of heterogeneous capillary PO_2, a complete breakdown in qualitative agreement between Voronoi polygons and some trapping regions is seen (Fig. 4(i)), despite the range of capillary partial pressures being restricted (20–30 mmHg) such that the variation in capillary oxygen levels was less than an order of magnitude. Nonetheless, many capillaries fail to supply any oxygen, implying null trapping region areas, while the corresponding Voronoi polygons remain unaffected.

5.4 Quantitative Correlations

5.4.1 The Area Correlation, $\mathcal{CC}$

Table 3 demonstrates a strong correlation between the areas of Voronoi polygons and trapping regions for all capillary distributions where homogeneous capillary PO_2 is considered. Generally, these data indicate that the highest area correlation ($\mathcal{CC}$) is seen in highly regular capillary distributions with uniform p_{cap}, with the lowest found in rarefied distributions. Although $\mathcal{CC}$ is high in all cases of capillary rarefaction, it is still slightly smaller compared to all other capillary distributions with uniform p_{cap}. In contrast, for the case of heterogeneous capillary PO_2, $\mathcal{CC}$ is substantially lower.

5.4.2 *The Normalized Means Δ_{mean}, $\cap_{\text{mean}}$ and Area Ratio $\mathcal{R}$*

These statistics have a trend correlated with heterogeneity, and are rather different for random and real capillary arrangements. The normalized mean of difference (Δ_{mean}) provides a measure of the degree of failure of Voronoi polygons to cover comparable areas to those of trapping regions, which increases with the degree of perturbation to capillary arrangements. Given uniform p_{cap}, the highest Δ_{mean} is observed in severe rarefaction.

The normalized mean of intersection ($\cap_{\text{mean}}$) and the mean ratio ($\mathcal{R}$) describe how well Voronoi polygons capture functional capillary supply of trapping regions, with values of unity for cases of a perfect match. Both these statistics decrease linearly with measures of heterogeneity and, for homogeneous p_{cap}, are lowest in the case of severe rarefaction.

5.4.3 *The Normalized Standard Deviations Δ_{std}, $\cap_{\text{std}}$, $\square_{\text{std}}$, $\bigcirc_{sd}$*

The normalized standard deviations remain small across nearly homogeneous distributions and increase with greater heterogeneity of capillary distribution, the highest values corresponding to the highest degree of heterogeneity, i.e. severe rarefaction, at least in the absence of capillary PO_2 heterogeneity. The trend in Δ_{std} illustrates that the spread of Voronoi polygon areas begins to differ extensively from that of the trapping regions for extreme cases of structural heterogeneity.

The measure $\cap_{\text{std}}$ further scrutinises this relationship by considering areas of the Voronoi polygons that overlap with trapping regions. The greater magnitude with increasing heterogeneity suggests that even though Voronoi polygons might cover comparable areas with trapping regions, the two-dimensional domains of capillary supply regions are increasingly different from trapping regions within the tissue domain, consistent with results in Figs. 4 and 6(b).

The dispersion in oxygenation areas, as measured by $\square_{\text{std}}$ and $\bigcirc_{\text{std}}$, remain very small for nearly homogeneous capillary distributions. However, both spread statistics begin to widen as structural heterogeneity is increased. In particular, the dispersion in Voronoi tessellation areas is found to be approximately double that of the trapping regions across all tissue heterogeneities, except in the case of perfect homogeneity where numerical error leads to a positive normalised standard deviation in trapping regions. Introducing functional heterogeneities (e.g. p_{cap}) has no effect on $\square_{\text{std}}$: only trapping regions are influenced by such changes as with a heterogeneous p_{cap} where $\bigcirc_{\text{std}} = 0.5615$, highlighting an advantage of trapping regions.

6 Discussion

Due to their practicality and ease of use, Voronoi polygons and Krogh cylinders are widely taken to represent capillary domains or supply areas in studies requiring an objective assessment of the capacity for oxygen delivery by diffusion (e.g. Egginton and Ross 1992; Egginton and Gaffney 2010; Popel 1989; Kreuzer 1982; Fletcher 1978; Goldman 2008; Hoofd 1992). Krogh cylinders, however, are inadequate for this role since they lead to non-physiological tissue voids and overlaps. In

contrast, a number of investigators (Egginton and Gaffney 2010; Hoofd et al. 1990; Wang and Bassingthwaitghte 2001) have observed that, for perfect structural symmetry and functional homogeneity, Voronoi polygons coincide with capillary supply regions. Whether this relationship is sufficiently accurate in less idealised and physiological scenarios is less clear. Hence, our present study considered the flux trapping region, which is a more general approximation for the capillary supply region, and examined the quality of Voronoi polygons in capturing capillary supply boundaries. We then consider when such polygons are appropriate to assess O_2 supply from capillary distributions within muscle tissue cross sections.

It is clear that Voronoi polygons may exaggerate capillary supply areas. A qualitative understanding of this emerges from considering that wherever there is a local decrease in capillary density, the associated supply areas calculated via trapping regions can be compensated by non-nearest neighbour capillaries. In contrast, Voronoi polygon area distributions for capillary supply areas implicitly assume that only the nearest (contiguous) capillaries can supply oxygen: thus compensation is restricted to a small number of capillaries, hence overestimating the tissue regions they may supply.

Despite this, Voronoi polygons and trapping regions nonetheless have the same qualitative shapes and overall quantitative distributions for uniformly perfused, non-rarefied systems regardless of the degree of structural asymmetry (see Table 3 and Figs. 4–6), assuming the tissue is maintained above the level of saturating oxygen uptake. Then the mean ratio of the Voronoi polygon area to the trapping region area remains above 85 % in the absence of noticeable capillary rarefaction. This remains true even for randomly distributed capillaries. These observations are also robust to variations in the adjustable parameters of the transport model, as illustrated in Appendix C, where we consider the non-dimensional capillary permeability and the dimensional capillary density. Thus, in the absence of extremes that are only associated with pathologies, our modelling predicts that Voronoi polygons provide a simple and accurate approximation of functional capillary supply under uniform capillary PO_2, e.g. during maximal sustainable activity.

This is in contrast to Wang and Bassingthwaighte's modelling conclusions (Wang and Bassingthwaitghte 2001), due to the latter's consideration of unphysiologically low capillary densities to facilitate mathematical analysis, which presented artefacts associated with the boundary conditions. However, with an increase in computing power and a generic formalism, we have been able to consider more representative capillary distributions and larger domains, including the use of a region of interest sufficiently far from the domain perimeter to remove boundary artefacts. Furthermore, the trapping regions statistics are insensitive to substantial variations in all the modelling parameters, as detailed in Appendix C, and thus share an attractive feature of Voronoi polygons of not requiring detailed parameter estimates.

However, increasing the degree of capillary rarefaction decreases the quality of Voronoi polygons as indices for the profile of tissue oxygenation. This is further validated by the rarefaction of a rat EDL muscle (Fig. 6 and Table 3), thus confirming the absence of methodological artifacts. In particular, rarefaction results in complex integral paths representing O_2 flux that cannot be accommodated within the purely geometrical construct of Voronoi polygons. This indicates that Voronoi polygons may

be of limited use and inaccurate in assessing capillary supply areas for pathological situations associated with capillary rarefication, such as hypertension (Greene et al. 1992), diabetes (Cosyns et al. 2008), and *vasculitides* (Thacker et al. 2010), and perhaps even for muscle tissues that are undergoing cellular modifications, such as localised fibre hypertrophy, which may become in effect locally rarefied. We re-emphasise here that rarefaction is a local phenomenon. Thus, any change in global parameters such as capillary density may not necessarily affect the degree of tissue rarefaction. In particular, a reduction in capillary density and oxygen consumption effectively impacts a change in parameters to which trapping regions are insensitive assuming $p > p_{\text{critical}}$. This means that the appropriateness of Voronoi tessellations in this case is dependent on the level of heterogeneity in capillary distribution, which is usually signified by the normalised standard deviation of Voronoi tessellation areas.

We further note that anatomical rarefactions differ from functional ones. While the physical removal of capillaries is captured by both trapping regions and Voronoi tessellations, a functional blockade of capillaries cannot be accommodated by Voronoi tessellations unless the non-functional capillaries are known a priori. Even in the latter case, the local O_2 feedback imposed by continuity of O_2 flux across capillary walls results in local minima at the walls of non-functional capillaries, whereas the anatomical removal of capillaries may not necessarily have the same effect. Due to this, trapping regions are anticipated to cover somewhat different areas in each of the above situations generating the discrepancy between the cases of rarefaction and non-uniform capillary PO_2.

Additionally and in agreement with previous observations (Egginton and Gaffney 2010; Wang and Bassingthwaitghte 2001), Voronoi polygons and trapping regions develop increasing differences as non-uniformity in capillary PO_2 is introduced. In contrast, trapping regions analyses can in principle incorporate differential capillary PO_2 levels without violating the modelling assumptions and, therefore, may be a useful tool in the presence of significant capillary functional heterogeneity. For instance, the influences of (1) large and differential variations in consumption rate for different muscle fibre types, (2) fibre type-dependent capillary density (Egginton et al. 1988), (3) fibre-size variations, and (4) myoglobin facilitation and hypoxia may accentuate these differences and will form the subject of subsequent studies.

Finally, the correlation between Voronoi polygon and trapping region areas is higher for the rat muscle cross section compared to randomly distributed capillaries. This suggests the anatomical capillary distribution is tightly regulated to prevent random regions of capillary clustering and rarefication. Hence, the correlations between Voronoi polygons and trapping regions may be more generally informative in physiological studies, likely reflecting local control of angiogenic foci on the length scale of fibre diameter, 50–100 μm (Badr et al. 2003).

In summary, while the Voronoi polygon approximation to trapping regions depends on tissue heterogeneity, it is nonetheless representative for uniform capillary O_2 tension and maximal oxygen uptake given the absence of rarefaction, while also exhibiting an insensitivity to model parameters. As such, measures of muscle capillary supply capacity based on Voronoi tessellations may be sensibly and reasonably used for normal tissue, though extremes in the underlying approximation of capillary supply area are slightly exaggerated. However, increases in heterogeneity associated

with capillary rarefaction or pathological variations in capillary O_2 tension, even with maximal perfusion, eventually lead to a breakdown in the accuracy of Voronoi polygons. Hence, more sophisticated measures of capillary supply capacity should be used to study structural or functional dysregulation in pathological situations. Furthermore, flux trapping regions may provide a representation of capillary supply regions that is more robust to the introduction of heterogeneity compared to Voronoi tessellations, though an experimental validation has yet to be performed.

Acknowledgements This research was supported by a studentship awarded to the first author by Kuwait University, Department of Mathematics. We thank the anonymous reviewers for valuable comments, insights, and suggestions that greatly improved the manuscript.

Appendix A: Mathematical Details

A.1 Uniqueness of Solution

Consider the partial differential equation for the oxygen partial pressure, p:

$$\nabla^2 p - \mu = 0 \quad \text{in } C, \tag{13}$$

$$\left.\frac{\partial p}{\partial r}\right|_{r=1} = 0, \qquad \mathbf{n}_i \cdot \nabla p = \kappa(\eta_i - p) \quad \text{on } \partial C_i, \tag{14}$$

where C is the unit disk, C_i is the ith circular capillary, and $\mathbf{n}_i$ is the normal *inward* to the ith capillary and outward to C. For every $i \in \{1, \ldots, N_c\}$, the boundary condition on ∂C_i is $\mathbf{n}_i \cdot \nabla p = \kappa(\eta_i - p)$. When the oxygen tension is higher inside capillaries ($p < \eta_i$) the flux is then outward to the capillary ($-\partial_r p > 0$), so that κ is positive. The solution is unique, as we now demonstrate.

Let $q := p - \tilde{p}$ for two possibly different solutions $p, \tilde{p}$ which satisfy Eq. (13). Thus, $\nabla^2 q = 0$ with boundary conditions $\mathbf{n}_i \cdot \nabla q = -\kappa q$ on capillaries and $\mathbf{n}_i \cdot \nabla q = 0$ on the unit circle. By Green's identity, we employ these boundary conditions to get

$$0 \le \int_C (\nabla q)^2 \, dA = \oint_{\partial C} q(\mathbf{n}_i \cdot \nabla q) \, ds - \int_C q \nabla^2 q \, dA = -\kappa \sum_i \oint_{\partial C_i} q^2 \, ds \le 0$$

and, therefore, $\int_C (\nabla q)^2 \, dA = 0$, which implies $q =$ is constant on C. Consequently, $\oint_{\partial C_i} q^2 \, ds = 0$ which implies $q = 0$ on all ∂C_i. Thus, $p - \tilde{p} = q = 0$ on C and the solution is unique.

A.2 Trapping Regions

Recall that the streamlines associated with the oxygen partial pressure, p, are the integral paths of the dynamical system

$$\frac{d\mathbf{x}}{ds} = -\nabla p, \tag{15}$$

and that the trapping region associated with a capillary is the area of the muscle reached by streamlines emerging from the capillary boundary. Below we assume that all capillaries act as oxygen sources with no regions on their boundaries where the oxygen flux is from the tissue into the blood compartment, unless explicitly stated otherwise. This is valid for all examples considered in the main text except non-uniform capillary PO_2. In addition, note that the trapping regions considered below will tessellate the domain, requiring that oxygen supply is sufficient to prevent anoxia; the latter is highly pathological and the required parameter regimes are not considered in this study.

A.3 Area of Trapping Regions

The trapping region $D_i \subseteq D$ of a capillary with centre $\mathbf{x}_i$, with outward pointing normal $\mathbf{n}_i$ is defined to be the union of the smallest domain satisfying

$$D_i = \{\mathbf{x} \in D \,|\, \mathbf{n}_i \cdot \nabla p = 0,\ \mathbf{x} \in \partial D_i\}. \tag{16}$$

Using by A_i to denote the area of the ith trapping region, D_i, we integrate Eq. (13) over this region to obtain

$$A_i = \frac{\kappa}{\mu} \oint_{\partial C_i} (\eta_i - p)\, ds, \tag{17}$$

where ds is the *anti-clockwise* parameterisation element around the capillary and the trapping region. Note that, for a fixed capillary radius ϵ, this further simplifies to

$$A_i = \frac{\epsilon\kappa}{\mu} \int_0^{2\pi} \big(\eta_i - p_\epsilon(\theta)\big)\, d\theta. \tag{18}$$

When any region of a capillary boundary acts as a sink, with an oxygen flux from the tissue into the blood compartment, the above equation for trapping region areas is not valid. This only occurs in our study for the case of non-uniform capillary PO_2, and then we observe that all such cases have *all* streamlines at the capillary boundary pointing away from the tissue and into the capillary interior. In this instance, the trapping region is of zero area, allowing the evaluation of numerous statistics in the main text even in the case of non-uniform capillary PO_2.

A.4 General Properties of the Trapping Regions

When $\nabla p = \mathbf{0}$, we have a stationary point in the phase plane diagram associated with Eq. (15). Given the above is a gradient dynamical system, the Jacobian matrix must be symmetric. In particular, a non-degenerate stationary point of this system is restricted to a dynamical system sink, source, or saddle (Guckenheimer and Holmes 1997) and neither periodic streamlines (limit cycles) nor homoclinic connections can exist in a gradient dynamical system (Guckenheimer and Holmes 1997; Hirsch and Smale 1974).

Furthermore, no source exists other than possibly on capillary boundaries: at an interior source point, both p_{xx} and p_{yy} are negative or zero, giving the contradiction

$0 \geq \nabla^2 p = \mu > 0$. Similarly, maxima may not occur on the domain boundary (the unit circle). In polar coordinates, a maximum on the boundary satisfies $p_\theta = 0$ and $p_{\theta\theta} \leq 0$. The boundary condition is $p_r = 0$ which, by Taylor expansion about $r = 1$, gives $p_{rr} \leq 0$. Then, as above, we have the contradiction $0 \geq \nabla^2 p = \mu > 0$. In addition, when no region of a capillary boundary acts as a sink, with instead the oxygen flux always from the capillary into the tissue, or vice-versa, no point on a capillary is a stationary point as $p_r \neq 0$.

Hence, when streamlines emanate from capillary boundaries, the fact there are no sources in the tissue implies, from the Poincaré–Bendixson theorem (Hirsch and Smale 1974) that a streamline within a trapping region can only approach a closed loop that is made up by hetero-clinic connections of dynamical system stationary points. In principle, these stationary points may be degenerate, and thus non-hyperbolic, but this is not observed in practice (and the appearance of non-hyperbolic stationary points would require mathematical precision in parameter values, with a concomitant sensitivity in model behaviour). Hence, we have that the trapping region boundaries are connections between the allowed hyperbolic stationary points, i.e. saddles to saddles or saddles to sinks, noting that sink-sink connections are inconsistent with Eq. (15). Furthermore, Wang and Bassingthwaighte (2001) have shown that only saddle-minimum hetero-clinic connections are possible on the boundary of a trapping region. This latter property, combined with stationary point hyperbolicity (and that stationary points are finite in number), as observed in practice, implies that Eq. (15) is a Morse–Smale gradient field (Guckenheimer and Holmes 1997), and thus the dynamical system is structurally stable (Palis and Smale 1970).

The above properties of gradient dynamical systems are used below for a numerical algorithm that calculates the trapping region boundary given that all capillaries act as oxygen sources with no regions on their boundaries where the oxygen flux is from the tissue into the blood compartment.

Appendix B: Numerical Computations

B.1 Finite Element Method for the Oxygen Partial Pressure

We solve Eqs. (13)–(14) to determine the oxygen partial pressure. This is accomplished by using the finite element method (see, for example, Reddy 1993). The mesh used was generated by the PDE toolbox provided by Matlab (The MathWorks Inc., Natick, MA). Adaptive meshing was used to improve the accuracy of the computed solution around capillaries to resolve areas of rapid changes in oxygen partial pressure gradients.

B.2 Streamlines

Streamlines were computed by numerically solving Eq. (15) via Heun's method. As frequent numerical evaluations of ∇p are required by this numerical solver, linear interpolation is called upon to provide approximate values within elements of the finite element solution.

B.3 Trapping Regions

As above, in discussing trapping region properties, we assume that the flux of oxygen on capillary boundaries always points into the tissue compartment. We have that each trapping region is delimited by a collection of heteroclinic connections of type saddle-minimum. Such orbits of Eq. (15) are estimated numerically as follows:

(1) The unstable manifolds emerging from each saddle point are determined within machine level tolerances exploiting the local Hartman–Grobman theorem for hyperbolic equilibrium points of dynamical systems (Guckenheimer and Holmes 1997).
(2) Integration proceeds until ending at a dynamical system sink, thus giving the saddle-sink connection.
(3) All these connections are determined and the resulting tessellation of the domain gives the trapping regions, each of which is identified with the capillary it encloses.

Appendix C: Dependence on Parameters

In the non-dimensionalised model, there are $N_c + 3$ parameters: κ, μ, ϵ and η_i for $i = 1, \ldots, N_c$. The non-dimensional metabolic demand, μ, determines how much O_2 is absorbed by the tissue, and the non-dimensional mass transfer coefficient or capillary permeability, κ, is a measure of the O_2 flux leaving the capillary. The areas of the trapping regions are given by Eq. (18) and so are ostensibly dependent on κ, μ, the non-dimensional capillary radius ϵ, the ith capillary non-dimensionalised partial pressure, η_i, and the solution p. Below, we consider uniform p_{cap} so that all the η_i are equal and denoted by η. For non-uniform capillary supply, there are no analogous simplifications in the parameter dependencies of the trapping regions; however, studying such complications is not our focus.

C.1 Streamlines and Trapping Regions Are Independent of the Non-dimensional Capillary Partial Pressure and Oxygen Uptake

We consider a re-scaling of the equations to show that trapping region areas and shapes are independent of μ, η, and a re-scaling of p.

Fixing κ, η and ϵ, we re-scale $\mu \mapsto \xi\mu$. Then let $\tilde{p}$ denote the solution of Eqs. (13)–(14) with parameters κ, $\eta_i = \eta$, ϵ, and $(\xi\mu)$. By uniqueness, the solution $\tilde{p}$ must satisfy $\tilde{p} = \xi p - \xi\eta + \eta$. This clearly satisfies Eq. (13) for the given parameter values, while direct differentiation gives $\nabla\tilde{p} = \xi\nabla p$. Thus, all no-flux boundary conditions and stationary points are unchanged because $\nabla p = 0 \Longrightarrow \nabla\tilde{p} = 0$ provided $\xi \neq 0$.

In addition, the streamlines and trapping regions, are unchanged as the streamline parameter may be rescaled to give

$$\nabla\tilde{p} = \xi\nabla p = -\xi\frac{d\mathbf{x}}{ds} = -\frac{d\mathbf{x}}{dt}, \qquad \frac{ds}{dt} := \xi.$$

Table 4 Statistics determined from areas of Voronoi polygons and trapping regions for the geometry of rat EDL muscle cross section as in plots 5(f) within the main text. Results for unperturbed and perturbed parameters are presented. We consider reducing the non-dimensional capillary permeability, κ, by factors of 2 and 4, and increasing the dimensional capillary density, ρ, by factors of 4 and 16. For a description of the above statistics, the reader is referred to the main text

Muscle image	Δ_{mean}	Δ_{std}	$\cap_{\text{mean}}$	$\cap_{\text{std}}$	$\mathcal{CC}$	$\square_{\text{std}}$	$\mathcal{R}$
Unperturbed parameters	0.1501	0.1548	0.9297	0.1764	0.9483	0.2529	0.9241
$\frac{\kappa}{4}$	0.1517	0.1551	0.9296	0.1768	0.9470	0.2529	0.9242
$\frac{\kappa}{2}$	0.1528	0.1553	0.9294	0.1770	0.9464	0.2529	0.9239
4ρ	0.1516	0.1553	0.9296	0.1768	0.9471	0.2529	0.9242
16ρ	0.1526	0.1551	0.9295	0.1771	0.9466	0.2529	0.9238

Integrating Eq. (13) over the trapping region gives

$$\tilde{A}_i = \frac{\kappa}{\xi\mu}\int_{\partial D_i} \mathbf{n}_i \cdot \nabla \tilde{p}\, ds = \frac{\kappa}{\xi\mu}\int_{\partial D_i} \mathbf{n}_i \cdot \nabla(\xi p)\, ds = A_i,$$

where the ξ cancel to give the same expression as Eq. (17). Thus, the modelling predictions do not depend on changes in μ, while holding other parameters fixed.

Instead, fix κ, ϵ, and μ, and re-scale $\eta \mapsto \zeta\eta$. Then $\tilde{p} = p - \eta + \zeta\eta$ satisfies Eqs. (13)–(14) with the rescaled value of the nondimensional capillary partial pressure, $\zeta\eta$. By analogous reasoning to the above, we have that the streamlines and trapping regions are unchanged.

C.2 Varying the Non-dimensional Capillary Permeability, κ, and the Capillary Density ρ

Analogous to Table 3 in the main text, Table 4 above presents statistical measures for the geometry of rat EDL muscle (see Fig. 4(f)), but with the non-dimensional capillary permeability, κ, reduced by factors of 2 and 4, reducing oxygen supply into the tissue. Note that there is not an extensive difference on comparison with the unperturbed case, highlighting an insensitivity to κ, though the agreement between the Voronoi polygons and trapping regions slightly reduces. This trend holds given the permeability and oxygen supply is sufficient that oxygen levels are sufficient for maximal uptake; analogous comments hold for variations in the dimensional capillary density ρ.

Note that the non-dimensional capillary radius, ϵ, depends on the dimensional value and the scaling used to non-dimensionalise. The latter length scale is $L = \sqrt{4N_c/\pi\rho}$, as discussed in Sect. 3.2 of the main text, where N_c is the number of capillaries in the non-dimensional unit disc and ρ is the dimensional capillary density. Thus, assuming the dimensional capillary radius does not vary between capillaries in the cross-section, varying ϵ is equivalent to varying ρ. Thus, the above observations of insensitivity also apply and more generally we have that the trapping region statistics used in the main text are robust to variations in the model parameters, at least in the case of uniform capillary PO_2.

References

Ahmed, S. K., Egginton, S., Jakeman, P. M., Mannion, A. F., & Ross, H. F. (1997). Is human skeletal muscle capillary supply modelled according to fibre size or fibre type? *Exp. Physiol.*, *82*, 231–234.

Altman, P. L., & Dittmer, D. K. (1971). *Respiration and circulation*, *Biological handbooks* (pp. 139–154). Federation of American Societies for Experimental Biology.

Badr, I., Brown, M., Egginton, S., Hudlicka, O., Milkiewicz, M., & Verhaeg, J. (2003). Differences in local environment determine the site of physiological angiogenesis in rat skeletal muscle. *Exp. Physiol.*, *88*, 565–568.

Batra, S., & Rakušan, K. (1991). Geometry of capillary networks in volume overloaded rat-heart. *Microvasc. Res.*, *42*, 39–50.

Batra, S., Rakušan, K., & Campbell, S. E. (1991). Geometry of capillary networks in hypertrophied rat-heart. *Microvasc. Res.*, *41*, 29–40.

Beard, D. A., & Bassingthwaighte, J. B. (2001). Modeling advection and diffusion of oxygen in complex vascular networks. *Ann. Biomed. Eng.*, *29*, 298–310.

Bentley, T. B., Meng, H., & Pittman, R. N. (1993). Temperature-dependence of oxygen diffusion and consumption in mammalian striated-muscle. *Am. J. Physiol.*, *264*, H1825–H1830.

Burrowes, K., Tawhai, M., & Hunter, P. (2004). Modeling rbc and neutrophil distribution through an anatomically based pulmonary capillary network. *Ann. Biomed. Eng.*, *32*, 585–595.

Christoforides, C., Laasberg, L. H., & Hedley-Whyte, J. (1969). Effect of temperature on solubility of o2 in human plasma. *J. Appl. Physiol.*, *26*, 56–60.

Clark, A. Jr., Federspiel, W. J., Clark, P. A. A., & Cokelet, G. R. (1985). Oxygen delivery from red cells. *Biophys. J.*, *47*, 171–181.

Clark, P. A., Kennedy, S. P., & Clark, A. J. (1989). Buffering of muscle tissue PO_2 levels by the superposition of the oxygen field from many capillaries. In *Oxygen transport to tissue Xl* (Vol. 248, pp. 165–174). New York: Plenum.

Cosyns, B., et al. (2008). Effect of streptozotocin-induced diabetes on myocardial blood flow reserve assessed by myocardial contrast echocardiography in rats. *Cardiovasc. Diabetol.*, *7:26*.

Degens, H., Turek, Z., Hoofd, L. J. C., Vanthof, M. A., & Binkhorst, R. A. (1992). The relationship between capillarization and fiber types during compensatory hypertrophy of the plantaris muscle in the rat. *J. Anat.*, *180*, 455–463.

Degens, H., Anderson, R. K., & Alway, S. E. (2002). Capillarization in skeletal muscle of rats with cardiac hypertrophy. *Med. Sci. Sports Exerc.*, *34*, 258–266.

Degens, H., Deveci, D., Botto-Van Bemden, A., Hoofd, L. J. C., & Egginton, S. (2006). Maintenance of heterogeneity of capillary spacing is essential for adequate oxygenation in the soleus muscle of the growing rat. *Microcirculation*, *13*, 467–476.

Degens, H., Kosar, S. N., Hopman, M. T. E., & de Haan, A. (2008). The time course of denervation-induced changes is similar in soleus muscles of adult and old rats. *Appl. Physiol. Nutr. Metab.*, *33*, 299–308.

Deveci, D., & Egginton, S. (2002). Muscle ischaemia in rats may be relieved by overload-induced angiogenesis. *Exp. Physiol.*, *87*, 479–488.

Dong, M. (1997). *Influence of aging on oxygen transport in the microcirculation of skeletal muscle*. Ph.D. thesis, Virginia Commonwealth University.

Ebina, T., Hoshi, N., Kobayashi, M., Kawamura, K., Nanjo, H., Sugita, A., Sugiyama, T., Masuda, H., & Xu, C. P. (2002). Physiological angiogenesis in electrically stimulated skeletal muscle in rabbits: characterization of capillary sprouting by ultrastructural 3-d reconstruction study. *Pathol. Int.*, *52*, 702–712.

Egginton, S. (1990). Numerical and areal density estimates of fiber type composition in a skeletal-muscle (rat extensor digitorum longus). *J. Anat.*, *168*, 73–80.

Egginton, S. (2002). Temperature and angiogenesis: the possible role of mechanical factors in capillary growth. *Comp. Biochem. Physiol., Part a Mol. Integr. Physiol.*, *132*, 773–787.

Egginton, S., & Gaffney, E. A. (2010). Tissue capillary supply—it's quality not quantity that counts! *Exp. Physiol.*, *95*, 971–979.

Egginton, S., & Ross, H. F. (1989). Quantifying capillary distribution in four dimensions. *Adv. Exp. Med. Biol.*, *248*, 271–280.

Egginton, S., & Ross, H. F. (1992). Planar analysis of tissue capillary supply. In *Society for experimental biology seminar series: Vol. 51. Oxygen transport in biological systems* (pp. 165–195). Cambridge: Cambridge University Press.

Egginton, S., Turek, Z., & Hoofd, L. (1988). Differing patterns of capillary distribution in fish and mammalian skeletal muscle. *Respir. Physiol.*, *74*, 383–396.

Egginton, S., Fairney, J., & Bratcher, J. (2001). Differential effects of cold exposure on muscle fibre composition and capillary supply in hibernator and non-hibernator rodents. *Exp. Physiol.*, *86*, 629–639.

Eggleton, C. D., Vadapalli, A., Roy, T. K., & Popel, A. S. (2000). Calculations of intracapillary oxygen tension distributions in muscle. *Math. Biosci.*, *167*, 123–143.

Ellsworth, M. L., Popel, A. S., & Pittman, R. N. (1988). Assessment and impact of heterogenities of convective oxygen transport parameters in capillaries of striated muscle: experimental and theoretical. *Microvasc. Res.*, *35*, 341–362.

Fletcher, J. E. (1978). Mathematical modeling of the microcirculation. *Math. Biosci.*, *38*, 159–202.

Gayeski, T. E. J., & Honig, C. R. (1988). Intracellular po2 in long axis of individual fibers in working dog gracilis muscle. *Am. J. Physiol.*, *254*, H1179–H1186.

Goldman, D. (2008). Theoretical models of microvascular oxygen transport to tissue. *Microcirculation*, *15*, 795–811.

Goldman, D., & Popel, A. S. (2000). A computational study of the effect of capillary network anastomoses and tortuosity on oxygen transport. *J. Theor. Biol.*, *206*, 181–194.

Gonzalez-Fernandez, J., & Atta, S. E. (1972). Concentration of oxygen around capillaries in polygonal regions of supply. *Math. Biosci.*, *13*, 55–69.

Greene, A. S., Tonellato, P. J., Zhang, Z., Lombard, J. H., & Cowley, A. W. Jr. (1992). Effect of microvascular rarefaction on tissue oxygen delivery in hypertension. *Am. J. Physiol.*, *262*, H1486–93.

Guckenheimer, J., & Holmes, P. J. (1997). *Nonlinear oscillations, dynamical systems, and bifurcations of vector fields* (Vol. 42). Berlin: Springer.

Hargreaves, D., Egginton, S., & Hudlicka, O. (1990). Changes in capillary perfusion induced by different patterns of activity in rat skeletal muscle. *Microvasc. Res.*, *40*, 14–28.

Heron, M. I., & Rakušan, K. (1994). Geometry of coronary capillaries in hyperthyroid and hypothyroid rat-heart. *Am. J. Physiol.*, *267*, H1024–H1031.

Hirsch, M. W., & Smale, S. (1974). *Differential equations, dynamical systems, and linear algebra*. San Diego: Academic Press.

Honig, C. R., & Gayeski, T. E. (1982). Correlation of o2 transport on the micro and macro scale. *Int. J. Microcirc. Clin. Exp.*, *1*, 367–380.

Hoofd, L. (1992). Updating the Krogh model: assumptions and extensions. In *Society for experimental biology seminar series: Vol. 51. Oxygen transport in biological systems* (pp. 197–229). Cambridge: Cambridge University Press.

Hoofd, L. (1995). Calculation of oxygen pressures in tissue with anisotropic capillary orientation. i. Two-dimensional analytical solution for arbitrary capillary characteristics. *Math. Biosci.*, *129*, 1–23.

Hoofd, L., Turek, Z., & Olders, J. (1989). Calculation of oxygen pressures and fluxes in a flat plane perpendicular to any capillary distribution. *Adv. Exp. Med. Biol.*, *248*, 187–196.

Hoofd, L., Olders, J., & Turek, Z. (1990). Oxygen pressures calculated in a tissue volume with parallel capillaries. *Adv. Exp. Med. Biol.*, *277*, 21–29.

Hudlicka, O., Brown, M., & Egginton, S. (1992). Angiogenesis in skeletal and cardiac muscle. *Physiol. Rev.*, *72*, 369–417.

Janacek, J., Cvetko, E., Kubinova, L., Travnik, L., & Erzen, I. (2011). A novel method for evaluation of capillarity in human skeletal muscles from confocal 3d images. *Microvasc. Res.*, *81*, 231–238.

Jürgens, K. D., Peters, T., & Gros, G. (1994). Diffusivity of myoglobin in intact skeletal muscle cells. *Proc. Natl. Acad. Sci. USA*, *91*, 3829–3833.

Karch, R., Neumann, F., Ullrich, R., Neumuller, J., Podesser, B., Neumann, M., & Schreiner, W. (2005). The spatial pattern of coronary capillaries in patients with dilated, ischemic, or inflammatory cardiomyopathy. *Cardiovasc. Pathol.*, *14*, 135–144.

Koyama, T., & Taka, A. (2010). Renal vasoconstriction in rats causes a decrease in capillary density and an increase in alkaline phosphatase expression in cardiac capillary nets. In E. Takahashi & D. F. Bruley (Eds.), *Advances in experimental medicine and biology: Vol. 662. Oxygen transport to tissue XXXI* (pp. 83–88).

Koyama, T., Xie, Z., Gao, M., Suzuki, J., & Batra, S. (1998). Adaptive changes in the capillary network in the left ventricle of rat heart. *Jpn. J. Physiol.*, *48*, 229–241.

Kreuzer, F. (1982). Oxygen supply to tissues: the Krogh model and its assumptions. *Experientia*, *38*, 1415–1426.

Krogh, A. (1919). The number and distribution of capillaries in muscles with calculations of the oxygen pressure head necessary for supplying the tissue. *J. Physiol.*, *52*, 409–415.

Mahler, M., Louy, C., Homsher, E., & Peskoff, A. (1985). Reappraisal of diffusion, solubility, and consumption of oxygen in frog skeletal muscle, with applications to muscle energy balance. *J. Gen. Physiol.*, *86*, 105–134.

Meng, H., Bentley, T. B., & Pittman, R. N. (1993). Myoglobin content of hamster skeletal muscles. *J. Appl. Physiol.*, *74*, 2194–2197.

Palis, J., & Smale, S. (1970). Structural stability theorems. In S. S. Chein & S. Smale (Eds.), *Proceedings of symposia in pure mathematics* (Vol. 14, pp. 223–231). Providence: Am. Math. Soc.

Popel, A. S. (1989). Theory of oxygen transport to tissue. *Crit. Rev. Biomed. Eng.*, *17*, 257–321.

Rakušan, K., & Turek, Z. (1985). Protamine inhibits capillary formation in growing-rat hearts. *Circ. Res.*, *57*, 393–398.

Rakušan, K., Flanagan, M. F., Geva, T., Southern, J., & Vanpraagh, R. (1992). Morphometry of human coronary capillaries during normal growth and the effect of age in left-ventricular pressure-overload hypertrophy. *Circulation*, *86*, 38–46.

Rakušan, K., Cicutti, N., Kazda, S., & Turek, Z. (1994). Effect of nifedipine on coronary capillary geometry in normotensive and hypertensive rats. *Hypertension*, *24*, 205–211.

Rakušan, K., Cicutti, N., & Kolar, F. (2001a). Cardiac function, microvascular structure, and capillary hematocrit in hearts of polycythemic rats. *Am. J. Physiol.*, *281*, H2425–H2431.

Rakušan, K., Cicutti, N., & Kolar, F. (2001b). Effect of anemia on cardiac function, microvascular structure, and capillary hematocrit in rat hearts. *Am. J. Physiol.*, *280*, H1407–H1414.

Reddy, J. N. (1993). *An introduction to the finite element method*. New York: McGraw-Hill.

Richardson, R. S., Noyszewski, E. A., Kendrick, K. F., Leigh, J. S., & Wagner, P. D. (1995). Myoglobin o2 desaturation during exercise. evidence of limited o2 transport. *J. Clin. Invest.*, *96*, 1916–1926.

Richardson, R., Newcomer, S., & Noyszewski, E. (2001). Skeletal muscle intracellular po2 assessed by myoglobin desaturation: response to graded exercise. *J. Appl. Physiol.*, *91*, 2679–2685.

Safaeian, N., Sellier, M., & David, T. (2011). A computational model of hemodynamic parameters in cortical capillary networks. *J. Theor. Biol.*, *271*, 145–156.

Salathe, E. P. (2003). Mathematical analysis of oxygen concentration in a two dimensional array of capillaries. *J. Math. Biol.*, *46*, 287–308.

Schumacker, P. T., Chandel, N., & Agusti, A. G. N. (1993). Oxygen conformance of cellular respiration in hepatocytes. *Am. J. Physiol.*, *265*, L395–L402.

Scott, G. R., Egginton, S., Richards, J. G., & Milsom, W. K. (2009). Evolution of muscle phenotype for extreme high altitude flight in the bar-headed goose. *Proc. R. Soc. B*, *276*, 3645–3653.

Secomb, T. W., Hsu, R., Park, E. Y. H., & Dewhirst, M. W. (2004). Green's function methods for analysis of oxygen delivery to tissue by microvascular networks. *Ann. Biomed. Eng.*, *32*, 1519–1529.

Sladek, T., Sladkova, J., Kolar, F., Papousek, F., Cicutti, N., Korecky, B., & Rakusan, K. (1996). The effect of at1 receptor antagonist on chronic cardiac response to coronary artery ligation in rats. *Cardiovasc. Res.*, *31*, 568–576.

Sullivan, S. M., & Pittman, R. N. (1984). In vitro o2 uptake and histochemical fiber type of resting hamster muscles. *J. Appl. Physiol.: Respir., Environ. Exercise Physiol.*, *57*, 246–253.

Suzuki, J., Kobayashi, T., Uruma, T., & Koyama, T. (2000). Strength training with partial ischaemia stimulates microvascular remodelling in rat calf muscles. *Eur. J. Appl. Physiol.*, *82*, 215–222.

Thacker, S. G., Berthier, C. C., Mattinzoli, D., Rastaldi, M. P., Kretzler, M., & Kaplan, M. J. (2010). The detrimental effects of ifn-alpha on vasculogenesis in lupus are mediated by repression of il-1 pathways: potential role in atherogenesis and renal vascular rarefaction. *J. Immunol.*, *185*, 4457–4469.

Tomanek, R. J., Aydelotte, M. R., & Butters, C. A. (1990). Late-onset renal-hypertension in old rats alters myocardial microvessels. *Am. J. Physiol.*, *259*, H1681–H1687.

Tomanek, R. J., Wessel, T. J., & Harrison, D. G. (1991). Capillary growth and geometry during long-term hypertension and myocardial hypertrophy in dogs. *Am. J. Physiol.*, *261*, H1011–H1018.

Turek, Z., Hoofd, L., & Rakušan, K. (1986). Myocardial capillaries and tissue oxygenation. *Can. J. Cardiol.*, *2*, 98–103.

Turek, Z., Kubat, K., Kazda, S., Hoofd, L., & Rakusan, K. (1987). Improved myocardial capillarization in spontaneously hypertensive rats treated with nifedipine. *Cardiovasc. Res.*, *21*, 725–729.

Turek, Z., Hoofd, L., Batra, S., & Rakušan, K. (1992). The effect of realistic geometry of capillary networks on tissue oxygen partial pressure in hypertrophied rat heart. In *Advances in experimental medicine and biology; oxygen transport to tissue XIV* (Vol. 317, pp. 567–572).

Wang, C. Y., & Bassingthwaitghte, J. B. (2001). Capillary supply regions. *Math. Biosci.*, *173*, 103–114.

Wilson, D. F., Rumsey, W. L., Green, T. J., & Vanderkooi, J. M. (1988). The oxygen dependence of mitochondrial oxidative-phosphorylation measured by a new optical method for measuring oxygen concentration. *J. Biol. Chem.*, *263*, 2712–2718.

Wüst, R. C. I., Jaspers, R. T., van Heijst, A. F., Hopman, M. T. E., Hoofd, L. J. C., van der Laarse, W. J., & Degens, H. (2009a). Region-specific adaptations in determinants of rat skeletal muscle oxygenation to chronic hypoxia. *Am. J. Physiol.*, *297*, H364–H374.

Wüst, R. C. I., Gibbings, S. L., & Degens, H. (2009b). Fiber capillary supply related to fiber size and oxidative capacity in human and rat skeletal muscle. In P. Liss, P. Hansell, D. F. Bruley, & D. K. Harrison (Eds.), *Advances in experimental medicine and biology: Vol. 645*. *Oxygen transport to tissue XXX* (pp. 75–80).